CRYSTAL GROWTH & DESIGN

pubs.acs.org/crystal

Article

Cationic Disorder in Co_2AlBO_5: Effects on Magnetic and Electrical Properties

Yulia S. Gokhfeld,* Natalia V. Kazak,* Anastasia S. Tarasova, Alexander D. Vasiliev, Evgeniy V. Eremin, Andrey A. Borus, Oleg A. Kondratev, Anna O. Belyaeva, and Sergey G. Ovchinnikov

Cite This: https://doi.org/10.1021/acs.cgd.4c00582

Read Online

ACCESS | Metrics & More | Article Recommendations | Supporting Information

ABSTRACT: Single crystals of Co_2AlBO_5 were synthesized using flux. The structural, magnetic, and electrical properties have been studied, with emphasis on cationic disorder effects. The Al^{3+} and Co^{2+} ions share four symmetry inequivalent sites. Large amplitudes of the displacement parameters for the M2 and M4 metal sites and the O4 oxygen site were found. The compound exhibits two magnetic transitions at T_1 = 41 K and T_2 = 20 K and shows a high crystallographic anisotropy. The random cationic distribution induces magnetic softness and an increase in electrical resistivity. The sources of the cationic disorder and the approach for controlling it are discussed.

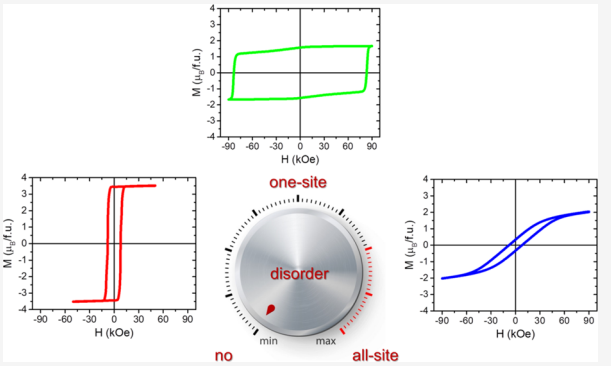

1. INTRODUCTION

The disorder is a driving force throughout many of the highest-profile phenomena of solid-state physics. Frustrations of exchange interactions play a central role in low-dimensional magnets.[1] Competing antiferromagnetic exchange interactions between localized magnetic moments so that all exchanges cannot be satisfied simultaneously can prevent magnetic ordering down to very low temperatures and may even stabilize unconventional forms of ordering, such as spin liquid or noncollinear magnetic structure.[2,3] The high-zT thermoelectric materials achieve reduced lattice thermal conductivity through disorder within the unit cell.[4] Recently, it was reported about an unprecedentedly low thermal conductivity in layered compound $AgCrSe_2$ due to disordered silver atoms over two tetrahedral sites and a large Seebeck coefficient.[5] Such a remarkable combination of properties leads to a thermoelectric figure of merit higher than 1 and opens the route to the discovery of efficient thermoelectric materials. In relaxors, the polarization is correlated on a local scale, resulting in the appearance of polar nanometer-sized regions (PNR) closely related to the structural and charge inhomogeneities. The PNRs generated from the disorder are found in all relaxors, whereas the structural or atomic origin may be different.[6−8]

Ludwigites with the general formula Me_3BO_5 belong to the family of intrinsically disordered systems.[9] These materials might be expected to exhibit structural disorder. One of the reasons is the atomic instability lying in the crystal structure itself, which contains cationic and anionic positions with a large displacement amplitude. Atomic instability is most pronounced in homometallic ludwigites and results in electronic and structural phase transitions in Fe_3BO_5. This phenomenon was extensively studied using X-ray and neutron diffraction methods, as well as Mössbauer spectroscopy.[10−12] Above T_{CO} = 283 K, the Fe2 cation presents a strongly anisotropic atomic displacement parameter along the rung Fe4−Fe2−Fe4, while below T_{CO}, this parameter drastically decreases, and the Fe2 cation is displaced toward Fe4, forming dimers alternating in a zigzag way along c-axis. These structural transformations are accompanied by a charge-order−disorder transition and the localization of an extra electron at the rung. Anomalies in the electrical resistivity and the semiconductor-semiconductor transition occur with decreasing activation energy. However, the atomic, charge, and structural stabilities have been found in Co_3BO_5 that have become the subject of intense discussions in recent decades.[13,14] By applying neutron powder diffraction, X-ray diffraction, X-ray absorption spectroscopy, heat capacity, electrical resistivity, and magnetic susceptibility measurements, as well as theoretical calculations in the framework of density functional theory (DFT), it was shown that the low-spin state of Co^{3+} ions prevents charge hopping, stabilizing structural and charge ordering and thereby avoiding structural phase transitions.[15−18] When heated above 500 K, the thermal energy becomes sufficient to overcome the

Received: April 27, 2024
Revised: August 13, 2024
Accepted: August 13, 2024

spin gap, and spin state crossover occurs. In Co_3BO_5, the interconnection between the electronic and lattice degrees of freedom is manifested in the coupled behavior of the electrical resistivity and thermal expansion. Thus, ludwigites exhibit a variety of physical phenomena, stemming from the delicate concert of trade-offs between structural order and disorder, charge ordering and disordering, and atomic stability and instability.

The great diversity of possible combinations of Me^{2+} and Me^{3+} ions provides an opportunity to study the intriguing electronic and magnetic properties of heterometallic ludwigites. Such systems can offer particularly attractive physical properties, including high crystallographic anisotropy, anomalous thermal expansion, magnetic dimensional crossover, and charge localization-delocalization phenomena. By substitution, it is possible to introduce sufficient disorder within the crystalline framework and to impact the system's ability to achieve an ordered state. Most of the research has focused on magnetic characterization, such as cascade phase transitions in Co_2FeBO_5,[19] Ni_2FeBO_5,[20] Cu_2MnBO_5,[21] and $Fe_{3-x}Mn_xBO_5$,[22] whereas the origin of cationic disorder remains to be investigated.

Al-substituted ludwigites possess the highest cationic disorder and are candidates for studying this effect. Medrano et al. reported on the emergence of ferrimagnetism at T_N = 57 K and the metamagnetic transition at 25 K in $Co_{2.38}Al_{0.62}BO_5$.[23] The magnetization, heat capacity, and dielectric constant measurements of Co_2AlBO_5 revealed that long-range magnetic order occurs at T_N = 42 K and that the superglass state is at T_G = 10.6 K.[24] Although Co_2AlBO_5 has been characterized from a magnetic point of view, there are discrepancies in both the interpretation of the magnetic ground state and the transition temperature itself. The present work undertakes the synthesis of a Co_2AlBO_5 single crystal by flux and the magnetic and electronic properties were studied, with an emphasis on highlighting how cationic disorder can give rise to unusual physical properties in this long-established class of materials. We used the inversion degree parameter as a means of characterizing disorder, and we suggest that this disorder might be tuned through the rich structural chemistry of this family.

2. EXPERIMENTAL METHODS

2.1. Synthesis. Single crystals of Co_2AlBO_5 were grown using a bismuth trimolybdate-based flux, in which Bi_2O_3 is strongly bonded to MoO_3, excluding the former entering the crystal. The system was: 71.3% mass [$Bi_2Mo_3O_{12}$ + Na_2O + 2.7·B_2O_3 + 0.1·CoO] + 28.7% mass [Co_2AlBO_5].

Flux with a weight of 30 g was prepared in a 100 cm^3 platinum crucible by sequential melting of B_2O_3, $Bi_2Mo_3O_{12}$, Co_3O_4, and Al_2O_3, and finally, the powder of Na_2CO_3 was added in portions at 1100 °C. The excess amount of B_2O_3 (20%) was determined through preliminary calcination at 400 °C and subsequent weighing. The crucible with melted solution was rapidly cooled to 1000 °C and kept for 6 h to ensure that the powder melted into a homogeneous solution. After that, the temperature was reduced to T_{cr} = 920 °C, followed by slow cooling at 4 °C/day. After 2 days, the growth was completed, and the liquid solution melt was poured out. The single crystals grown on the walls and at the bottom of the crucible were separated by etching in a 20% solution of nitric acid. The crystals are well cut into rectangular prisms of black color with a shiny surface (Figure S1). The thin crystals are brown in color. The crystal length is up to 7 mm, and the cross-section size is about 0.4 × 0.4 mm^2. In the temperature range of (T_{cr} − 30) °C < T < T_{cr}, the Co_2AlBO_5 ludwigite is only crystallizing phase. At T < 890 °C, blue-violet crystals were observed and identified as pyroborate.

2.2. Structure Determination. A single crystal of Co_2AlBO_5 was selected for structure determination. X-ray diffraction patterns were collected at 296 K using a SMART PHOTON II single-crystal diffractometer (Bruker AXS) equipped with a PHOTON II CCD-detector, graphite monochromator, and Mo Kα radiation source. The structure was solved by direct methods using the SHELXT program.[25] The structure refinement was carried out by least-squares minimization in the SHELXL program using the anisotropic thermal parameters of all atoms.[26]

2.3. Composition Analysis. To study the chemical composition of the grown crystals, X-ray microfluorescence analysis (micro-XRF) was carried out. The "Area" mode was used for quantitative analysis using an M4 TORNADO X-ray spectrometer (Bruker), which allows for mapping of the selected areas of the sample surface. According to a given number of points, statistics are collected and averaging and quantitative analysis are used for the determination of the concentrations of different chemical elements. The one-point mode measurements were carried out with an accumulation time of 150 s. The content-determining error of the main elements was ≈0.5%, and impurities with a content of less than 0.5% were determined qualitatively.

2.4. Magnetic Measurements. For magnetic measurements, a single crystal of 0.48 mg was selected. The sample was preliminarily oriented by using a single-crystal diffractometer and placed in a sample holder with the help of a microscope. The *dc* magnetization measurements were performed using a Quantum Design Physical Properties Measurement System (PPMS) with a maximum field of 90 kOe. The external magnetic field was applied directed parallel to the *b*- and *c*-axes.

2.5. Electrical Resistivity Measurements. Owing to the large size and rectangular shape of the grown crystals, it was possible to measure the electrical resistivity of Co_2AlBO_5 ludwigite. The measurements were performed in the temperature range of 400−870 K using an experimental setup for thermo-power and resistivity measurements.[27] The DC resistivity was measured along the *c*-direction with a standard four-point configuration. The heating/cooling rate was 6 K/min.

3. RESULTS

3.1. Crystal Structure. The structure refinement parameters and detailed crystallographic data are summarized in Table 1. The fractional coordinates, site occupation factors, anisotropic displacement parameters, and main bond lengths are listed in the Supporting Information (Tables S1−S4). Co_2AlBO_5 crystallizes in orthorhombic symmetry, in the space group *Pbam* (No.55), and the lattice parameters are in good agreement with those reported earlier.[23,24,28] There are four symmetry inequivalent metal sites, M1 (*2a*), M2 (*2d*), M3 (*4g*), and M4 (*4h*); one boron site, B (*4h*); and five oxygen sites, O1−O5 (*4g*, *4h*) (Figure 1a). The Co and Al ions share four metal sites with occupation factors Co:Al = 0.78:0.22 (M1), 0.53:0.47 (M2), 0.86:0.14 (M3), and 0.50:0.50 (M4). The refined formula $Co_{2.02}Al_{0.98}BO_5$ is in agreement with the X-ray microfluorescence analysis results, showing the high uniformity of the metal ion distribution (Figure S2). The ludwigite crystal structure can be presented as a framework consisting of octahedral layers in the *bc*-plane built on the M1, M2, and M3 sites, which are separated along the *a*-axis by $M4O_6$ octahedra and BO_3 triangles.

The local octahedral distortions were estimated through the calculations of the main component of the electrical field gradient tensor (V_{zz}).[29] The local oxygen coordination of metal ions exhibits two types of highly distorted octahedra: $M1O_6$ and $M3O_6$ preferably occupied by Co^{2+} ions (78 and 86%, respectively) have coordination, forming axially compressed octahedra and showing the largest values of V_{zz} (0.210 and

https://doi.org/10.1021/acs.cgd.4c00582
Cryst. Growth Des. XXXX, XXX, XXX−XXX

Table 1. Crystal Data and Structure Refinement for Co_2AlBO_5

	Crystal Data
space group, Z	*Pbam*(55), 2
size (mm^3)	0.420 × 0.220 × 0.190
T (K)	296
a (Å)	9.2072(3)
b (Å)	12.0676(4)
c (Å)	3.00170(10)
V ($Å^3$)	333.515(19)
D_x (mg/m^3)	4.694
μ (mm^{-1})	2.645
	Data Collection
wavelength	Mo Kα, λ = 0.71073 Å
measured reflections	6803
independent reflections	1036
reflections with $I > 2\sigma(I)$	851
absorption correction	multiscan
R_{int}	0.0330
$2\theta_{max}$ (deg)	75.96
H	−15 → 15
K	−20 → 20
L	−5 → 5
	Refinement
$R[F^2 > 2\sigma(F^2)]$	0.0269
$wR(F^2)$	0.0622
S	1.171
weight	$w = 1/[\sigma^2(F_o^2)] + (0.0186P)^2 + 0.3149P$

0.233 e/Å^3, respectively). On the contrary, the $M2O_6$ and $M4O_6$ octahedra are slightly distorted (V_{zz} = 0.076 and −0.030 e/Å^3, respectively). The reason for the difference is, obviously, the different boron coordination: four boron atoms coordinate the M1 and M3 sites and only two ones coordinate the M2 and M4 sites, causing considerable elongation of the appropriated Me−O bond length (Table S3).

3.2. Magnetic Properties. Figure 2 displays the temperature-dependent magnetization curves of the Co_2AlBO_5 single crystal in the field of 600 Oe directed along the *b*- and *c*-axes. The *dc* magnetization along the *b*-axis shows a maximum at T_1 = 41 K, which is close to the value of T_N = 42 K obtained by Kumar et al.,[24] and can be attributed to the onset of long-range magnetic order. Below T_1, a progressive divergence of the FC and ZFC curves is observed. A low-temperature magnetic

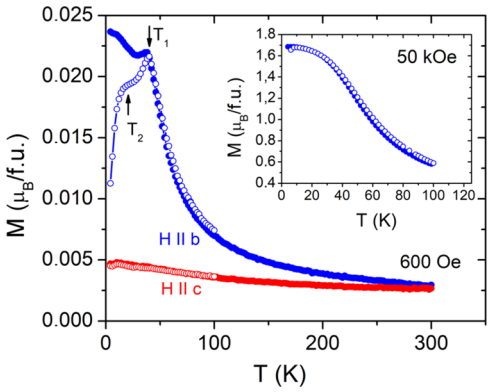

Figure 2. Temperature-dependent *dc* magnetization curves of Co_2AlBO_5 measured in a field of 600 Oe along the *b*- and *c*-axes. The full and empty symbols denote the FC and ZFC measurement regimes, respectively. The magnetic transitions are indicated by arrows. Inset: FC magnetization vs temperature measured along the *b*-axis in a field of 50 kOe.

anomaly occurs near T_2 = 20 K, which is somewhat higher than that at T_G = 10.6 K.[24] In high magnetic fields, the difference between the FC and ZFC curves rapidly decreases and the anomaly at T_1 is smeared and becomes indistinguishable against the growing ferromagnetic moment in a field of 50 kOe (inset to Figure 2). Importantly, the magnetic transitions are clearly identified in the magnetization curves along the *b*-axis, and almost no transitions are visible along the *c*-axis. At low temperatures, the magnetic moment along the *c*-axis is almost an order of magnitude smaller than that along the *b*-axis. This behavior indicates the high crystallographic anisotropy inherent in cobalt-containing ludwigites, which is due to the large single-ion anisotropy of Co^{2+} ions.[15,17,30]

At high temperatures (T > 150 K), the susceptibility follows a Curie−Weiss behavior and the data can be approximated by the sum of a temperature-independent term χ_0 and the Curie−Weiss term $\chi_{CW} = C/(T - \theta)$ (Figure 3). Fitting the data yields the parameters listed in Table 2. The obtained values of χ_0 are in good agreement with the summation of Pascal's constants for the ions constituting Co_2AlBO_5 ($\chi_{dia} = -0.61 \times 10^{-4}$ emu/mol)[31] and the van Vleck contribution of Co^{2+} ions in octahedral coordination ($\chi_{vV} = 12 \times 10^{-3}$ emu/mol).[32,33] Negative values of the Weiss temperature θ indicate the predominance of antiferromagnetic interactions. The exper-

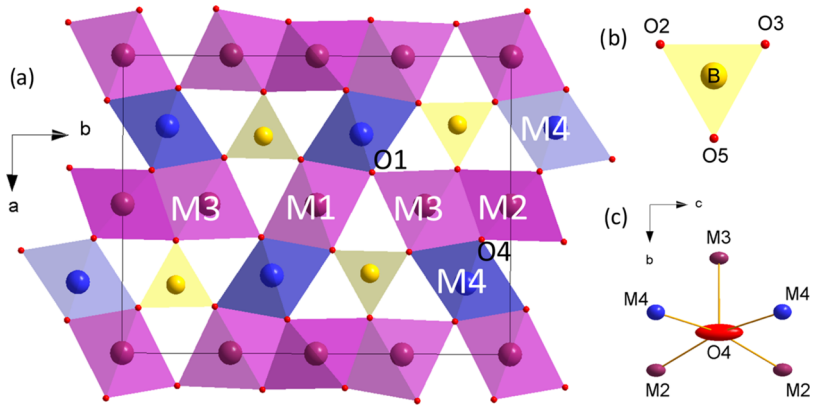

Figure 1. (a) Crystal structure of Co_2AlBO_5 in *ab*-projection. The inequivalent metal sites *2a*, *2d*, *4g*, and *4h* are numbered as M1, M2, M3, and M4, respectively. (b) BO_3-triangle. (c) Ellipsoid of thermal vibrations of the O4 atom surrounded by metal atoms.

https://doi.org/10.1021/acs.cgd.4c00582
Cryst. Growth Des. XXXX, XXX, XXX−XXX

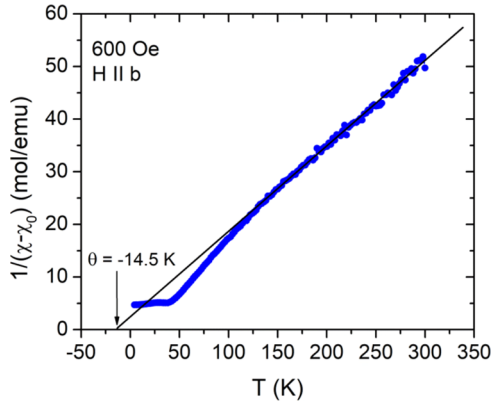

Figure 3. Temperature dependence of the inverse magnetic susceptibility $(\chi - \chi_0)^{-1}$ of the Co_2AlBO_5 single crystal for the H parallel b-axis. The straight line represents the Curie–Weiss fit.

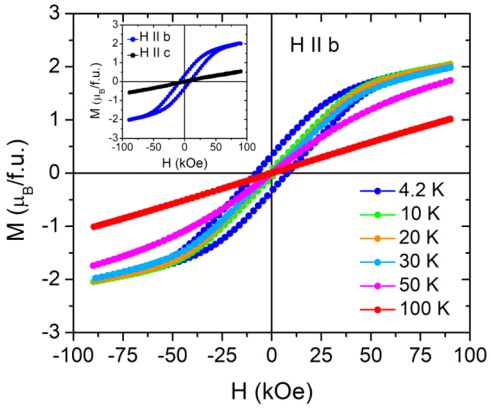

Figure 4. Field dependencies of the magnetization of the Co_2AlBO_5 single crystal over a temperature range of 4.2–100 K in the b-direction. The inset shows the hysteresis loops measured at T = 4.2 K and an external field applied along the b- and c-directions.

imental data deviate significantly from the Curie–Weiss fit at T < 150 K. The progressively increasing relevance of the antiferromagnetic correlations upon cooling leads to the onset of magnetic order at T_1. The Curie constant C yields an effective magnetic moment μ_{eff}^{b} = 7.04 ± 0.05 μ_B per formula unit, which corresponds to a moment of 4.97 ± 0.02 μ_B per Co^{2+} ion. The obtained value is in agreement with those for cobalt borates (μ_{eff} = 4.0–5.2 μ_B)[17] and exceeds the spin-only one, 3.87 μ_B. One can conclude that in Co_2AlBO_5 under consideration, the Co^{2+} ions are in the high-spin state with a significant unquenched orbital moment. The μ_{eff}^{c} value is depressed, implying strong magnetic anisotropy. The presence of some Co^{3+} ions in the $Co_{2.38}Al_{0.62}BO_5$ sample[23] gives an uncertainty in the effective moment value due to the lack of information about their spin state. Nevertheless, an estimated value of μ_{eff} per Co ion of 5.15 μ_B still falls within the range of the expected values. The magnetic moment of 3.5 μ_B reported for the Co_2AlBO_5 sample in ref 24 is smaller than that obtained in the present work.

The field dependences of the magnetizations of Co_2AlBO_5 measured for two directions of the external fields are shown in Figure 4. For the field applied along the c-direction, the magnetization curves are linear at all temperatures as expected for the antiferromagnet, while for the b-direction, the magnetization curves show temperature-induced evolution (inset to Figure 4). The high-field branches of the b-axis $M(H)$ are not saturated and have a slope, probably due to an antiferromagnetic component. At $T < T_1$, all curves tend to the same high-field limit (~2.0 μ_B/f.u.), assuming the presence of a magnetically disordered sublattice, which is affected by the ordered one. At $T < T_2$, the hysteresis loop opens, indicating that a noncompensated magnetic moment appears. The magnetic structure of ludwigites is complex and, in the first approximation, contains four magnetic sublattices assigned to inequivalent metal sites. The bulk magnetization is the sum of the partial contributions of the magnetization sublattices. The shape of the hysteresis loop reflects the dilution degree of these sublattices by nonmagnetic Al^{3+} and can differ for different samples.[23,24] The coercive field H_c increases as the temperature decreases, with a maximal H_c of ≈8.0 kOe at 4.2 K.

3.3. Electrical Resistivity. The electrical resistivity of the Co_2AlBO_5 single crystal as a function of the temperature is shown in Figure 5. At room temperature, the sample resistivity

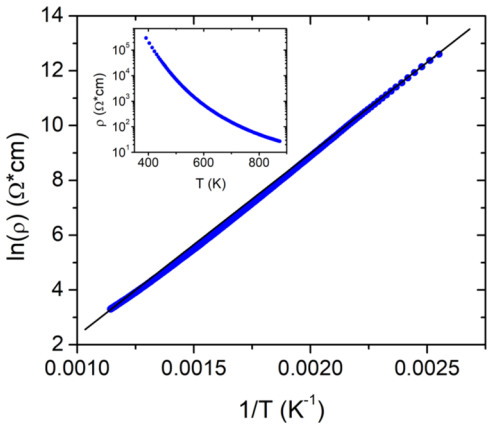

Figure 5. Resistivity of the Co_2AlBO_5 single crystal as a function of the inverse temperature. The black solid line is a linear approximation. The inset shows the temperature dependence of the electrical resistivity.

is extremely large. In fact, up to T = 400 K, the resistivity cannot be accurately measured. Above this temperature, the resistivity becomes measurable and decreases by approximately 4 orders of magnitude as the temperature increases to 870 K. Assuming that the high-temperature conductivity is due to thermally activated hopping of the carriers, the relation between the electrical resistivity and the inverse temperature is linear and yields an activation energy E_a = 0.57 ± 0.01 eV. Note that Co_3BO_5 undergoes two electronic transitions: the low- to high-spin-state transition of Co^{3+} at T_s = 500 K, followed by the semiconductor-semiconductor transition at T_{el}

Table 2. Magnetic Parameters of Co_2AlBO_5 Extracted in the Paramagnetic Phase

	χ_0 (emu/mol)	C (emu·K/mol)	μ_{eff} (μ_B/Co^{2+})	θ (K)
b-axis	(7.4 ± 0.5) × 10^{-3}	6.2 ± 0.1	4.97 ± 0.02	−14.5 ± 0.5
c-axis	(19 ± 1.0) × 10^{-3}	1.8 ± 0.3	2.68 ± 0.20	−27.0 ± 1.0

https://doi.org/10.1021/acs.cgd.4c00582
Cryst. Growth Des. XXXX, XXX, XXX–XXX

Table 3. Site Occupancies for the Four Inequivalent Metal Sites in Cobalt−Aluminum Ludwigites[a]

M1	M2	M3	M4	refs
Co (88%) + Al (12%)	Co (67%) + Al (33%)	Co (100%)	Co (60%) + Al (40%)	23
Co (81%) + Al (19%)	Co (55%) + Al (45%)	Co (70%) + Al (30%)	Co (46%) + Al (54%)	24
Co (78%) + Al (22%)	Co (53%) + Al (47%)	Co (86%) + Al (14%)	Co (50%) + Al (50%)	p.w.

[a]The destinations of the metal sites are consistent with those in the present work (p.w.) and are shown in Figure 1.

= 700 K, with a significant decrease in the activation energy from E_a = 0.50 ± 0.02 to 0.28 ± 0.02 eV.[17] The Co_2AlBO_5 resistivity data obtained within the same temperature interval did not reveal any anomalies in the $\rho(T)$ curve.

4. DISCUSSION

The compound under investigation inherited the main distinctive property of the Co-containing borates: strong magnetocrystalline anisotropy, the source of which is the large single-ion anisotropy of Co^{2+} ions. The analysis of the local distortions showed that Co^{2+} ions are coordinated by strongly distorted oxygen octahedra. If the symmetry of the crystal field is not cubic, the ground state of Co^{2+} ions is described, taking into account the spin−orbit coupling, by two Kramers doublets separated by about 100 cm^{-1}. At high temperatures, the system is characterized by the effective spin S = 3/2 and a small orbital contribution, which corresponds to an effective moment of about 4.97 μ_B. The population of the lowest Kramers doublet at low temperatures leads to an orbital contribution from the nearest level and a large anisotropy of the g-factor.

Although the temperature of the magnetic phase transition T_1 = 41 K almost does not change compared to that of Co_3BO_5 (T_N = 42 K[15]), the aluminum substitution effect is clearly identified through the appearance of an additional transition under cooling (T_2 = 20 K). The frequency-dependent behavior of the low-temperature anomaly confirmed by the results of the imaginary part of the *ac* susceptibility has been attributed to the spin-glass transition.[24] It is worth noting that similar behavior as well as bifurcation of the ZFC and FC magnetizations are also expected from the formation of domain walls in the ordered magnetic phase or from the spin-reorientation transition (metamagnetic transition, for instance, ref 23). Therefore, the nature of the low-temperature transition is still an open issue.

The hysteresis loop opening and rapid growth of the magnetic moment along the *b*-axis are probably due to the reorientation of one or several magnetic sublattices, which are weakly antiferromagnetically coupled, or their magnetic ordering. The diamagnetic dilution apparently results in the weakness of magnetic couplings, which the external magnetic field is capable of overcoming. The magnetically diluted sublattices either remain in a paramagnetic state below T_1 or make a small contribution to the magnetic order due to weak antiferromagnetic correlations. The difference in the magnetic behaviors, including the temperatures of the magnetic phase transitions, probably originates from the difference in the cationic distribution. These distributions are listed in Table 3. The cationic distribution of Co_2AlBO_5 determined in the present work is very close to that reported by Kumar et al.[24] The occupation of the M3 site by the Al atoms should induce a significant dilution of the M3-M1-M3 magnetic unit possessing the strongest antiferromagnetic coupling and, as a consequence, the weakness of the superexchange interactions. In contrast, the filling of the M3 site by magnetic Co^{2+} ions favors strengthening of the superexchange interactions, increasing the magnetic ordering temperature (T_N = 57 K[23]).

From an experimental viewpoint, cationic disorder has a number of observable consequences. A comparison of Co_2AlBO_5 with the isostructural orthoborates Co_3BO_5 and $Co_{2.5}Ge_{0.5}BO_5$ could be very helpful for understanding this effect. In terms of cationic disorder, Co_3BO_5 is a rare example of a no-disorder compound, whereas $Co_{2.5}Ge_{0.5}BO_5$ and Co_2AlBO_5 are the analogues of the one-site and all-site disorder compounds. In $Co_{2.5}Ge_{0.5}BO_5$, the Ge^{4+} and Co^{2+} ions share the M4 site in the ratio of Co:Ge = 0.5:0.5, making this site structurally disordered. The magnetically active Co^{2+} ions directly participate in the establishment of long-range antiferromagnetic order instead of the nonmagnetic LS Co^{3+} ions in Co_3BO_5, providing exchange interactions between adjacent $[Co^{2+}O_6]_\infty$-layers (M1, M2, and M3 sites). The antiferromagnetic order onsets at a high temperature (T_N = 84 K). In Co_2AlBO_5, all metal sites are structurally disordered, and magnetic order appears at a much lower temperature, T_1 = 41 K. The second magnetic transition occurs at T_2 = 36 K for germanium and 20 K for aluminum samples. The T_2 value is seemingly affected by the cationic distribution, as well.

Perhaps the most important effect of cationic disorder is the change in magnetic permeability, which transforms toward extraordinary magnetic hardness in the Ge-substituted sample and toward significant softness in the Al-substituted sample (Figure 6). To study this effect, we have carried out magnetization measurements on single crystals under the same temperature, field, and magnetic field orientation conditions. The $H_c{}^bM_r$ parameter, where $H_c{}^b$ is the coercive field along the *b*-axis and M_r is a remanent magnetization, is designed to describe a mechanism of 180° domain walls and equals 3.98 × 10^6 G^2 (T = 4.2 K) for Co_3BO_5,[15] 1.32 × 10^7 G^2 (T = 6 K) for $Co_{2.5}Ge_{0.5}BO_5$,[30] and only 3.02 × 10^5 G^2 (T = 4.2 K) for Co_2AlBO_5. Thus, the all-site cationic disorder induces the compound to become magnetically soft, while the

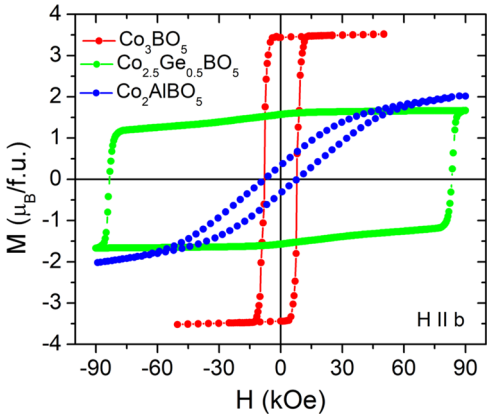

Figure 6. Hysteresis loops measured along the *b*-axis for Co_3BO_5 (T = 4.2 K),[15] $Co_{2.5}Ge_{0.5}BO_5$ (T = 6 K),[30] and Co_2AlBO_5 (T = 4.2 K).

https://doi.org/10.1021/acs.cgd.4c00582
Cryst. Growth Des. XXXX, XXX, XXX−XXX

Table 4. Bond Valence (v.u.) Analysis for Co_2AlBO_5[a]

	M1	M2	M3	M4	B	∑	∑/C.N.[b]
O1	0.445 $\frac{\times1\rightarrow}{\times2\downarrow}$		0.512 $\frac{\times1\rightarrow}{\times1\downarrow}$	0.516 $\frac{\times2\rightarrow}{\times2\downarrow}$		1.989	0.497
O2			0.306 $\frac{\times2\rightarrow}{\times2\downarrow}$	0.416 $\frac{\times1\rightarrow}{\times1\downarrow}$	0.953 $\frac{\times1\rightarrow}{\times1\downarrow}$	1.981	0.495
O3	0.322 $\frac{\times2\rightarrow}{\times4\downarrow}$			0.392 $\frac{\times1\rightarrow}{\times1\downarrow}$	1.008 $\frac{\times1\rightarrow}{\times1\downarrow}$	2.044	0.511
O4		0.385 $\frac{\times2\rightarrow}{\times4\downarrow}$	0.375 $\frac{\times1\rightarrow}{\times1\downarrow}$	0.349 $\frac{\times2\rightarrow}{\times2\downarrow}$		1.843	0.369
O5		0.433 $\frac{\times1\rightarrow}{\times2\downarrow}$	0.303 $\frac{\times2\rightarrow}{\times2\downarrow}$		0.995 $\frac{\times1\rightarrow}{\times1\downarrow}$	2.034	0.509
	2.178	2.406	2.105	2.538	2.956		

[a]The calculation was carried out for cobalt ions with R = 1.692 and R_0 = 0.37.[37] [b]C.N., coordination number.

one-site disorder provides magnetic hardness. Such systems are assumed to allow a mechanism for "switching" states between magnetically hard and soft materials through the cation distribution.

The effect of the random distribution of Co and Al is quite obvious, and these inhomogeneities can act as barriers to mobile charge carriers. The obtained resistivity is about 2 orders of magnitude greater than the reported value for Co_3BO_5.[18] The introduction of Al^{3+} "cuts through" the superexchange $Co^{2+}-O-Co^{2+}$ network, which restricts the movement of charge carriers. The hopping mobility through the $Co^{2+}-O-Al^{3+}$ network becomes difficult. As a result, the hopping mobility decreases, and hence, the resistivity increases.

In addition, charge carrier localization is supposed to yield a noticeable contribution to the conductivity. The band structure calculations in the DFT+U framework showed that at low temperatures, Co_3BO_5 is an insulator with a band gap of 1.4 eV.[17] The band gap for Co_2AlBO_5 is estimated to be $E_g = 2E_a = 1.14 \pm 0.01$ eV, which is very close to that for Co_3BO_5, implying that the electronic structure near the Fermi level has common features.

With respect to the origin of the cationic disorder in the ludwigites, clear peculiarities are evident. The M2 and M4 positions are most structurally disordered (Table 3). This is consistent with the large amplitudes of the displacement parameters U_{eq}(M2) = 0.00691(19) and U_{eq}(M4) = 0.00656(15) Å^2 (Table S1). As above-mentioned, in Fe_3BO_5, the atomic instability of the Fe2 position leads to an isostructural phase transition with a doubling of the lattice parameter c, accompanied by charge ordering.[12] In Co_3BO_5, the Debye–Waller coefficients σ^2 obtained using single-crystal X-ray diffraction data showed enhanced atomic disorder associated with the M4 site and the oxygen site connecting M2 and M4 at the spin-crossover temperatures.[34] Several works are only available on the temperature-dependent X-ray diffraction study of heterometallic ludwigites, which have shown that the crystal structure is stable with decreasing temperature and that symmetry remains (orthorhombic *Pbam* for Co_2AlBO_5[24] and monoclinic $P2_1/c$ for Cu_2CrBO_5[35]). However, in Co_2AlBO_5, anomalous behavior of the lattice parameters is observed near the Neel temperature and 150 K. The first anomaly can be attributed to spin–lattice interactions, whereas the origin of the other one is unclear. It is important to note that in heterometallic ludwigites the effects of atomic instability, although suppressed by cationic disorder, are still present and can manifest themselves upon cooling due to the weakening of thermal vibrations of oxygen atoms.

Among the five symmetry inequivalent oxygen atoms, three, namely, O2, O3, and O5, belong to a BO_3-triangle (Figure 1b), forming a rigid anionic framework, whereas O1 and O4 have relative freedom for displacement. The largest equivalent atomic displacement parameter is for O4 connecting the M2 and M4 sites: U_{eq}(O4) = 0.0225(5) Å^2 (Table S2). The ellipsoid of the thermal vibrations of the O4 atom is elongated in the direction of the linkage with the equivalent oxygen atom, i.e., along the share edge and coinciding with the c-direction (Figure 1c). The atomic instability of the O4 probably results from its unique cationic environment: the coordination number of O4 is five (five metal atoms) rather than four, as is the case for O1 (four metal atoms) or for O2, O3, and O5 (three Me atoms and one B atom) (Table 4 and Figure 1c). The bonds to 2 × M2, M3, and M4 supply 1.843 valence units (v.u.) to O4 or 0.369 v.u. per bond only, which is much less than those for other anions (0.495–0.511 v.u.) and compatible with the long mean bond ⟨O4–Me⟩ = 2.061 Å. The ability of O4 to shift leads to the lengthening/shortening of the corresponding Me–O4 bonds. As a result, the local symmetry of the coordination octahedra $M2O_6$ and $M4O_6$ changes, adapting to the requirements of the substitution ion. These sites are primarily filled by the substitutional ions, including the Jahn–Teller Cu^{2+} or Mn^{3+}.[20−24,28,36]

Finally, it is useful to discuss the issue of disorder control. Analogous to the spinel structure, in ludwigites, the cation distribution can be characterized by the so-called degree of inversion x, which is defined as the fraction of divalent metal ions at the octahedral M4 site

$$[Me^{2+}_{2-x}Me^{3+}_{x}]^{M1,M2,M3}(Me^{2+}_{x}Me^{3+}_{1-x})^{M4}BO_5$$

In this formula, the square brackets and parentheses denote the ions belonging to the octahedral layers (M1, M2, and M3 sites) or to the spacer between them (M4 site), respectively. The x = 0 corresponds to structurally ordered ludwigite, for instance, Co_3BO_5 with $[Co^{2+}O_6]_\infty$ octahedral layers and LS Co^{3+} ions located between them. An x = 1 yields inverse ludwigite with divalent ions at the M4 site, and the divalent and trivalent ions are distributed over the layer in equal proportions. The inversion degree of x = 2/3 corresponds to random ludwigite since divalent and trivalent ions are randomly distributed among both octahedral layers and M4 sites, and the number of divalent ions is double that of trivalent ions. The experimentally defined cation distribution has a rather wide range, yet never exceeds the random limit (Figure 7).

In ludwigites, the ionic radii relation between divalent and trivalent cations $r_i(Me^{2+})/r_iMe^{3+} \geq 1$ is always the case, suggesting that this parameter, although important, does not

https://doi.org/10.1021/acs.cgd.4c00582
Cryst. Growth Des. XXXX, XXX, XXX−XXX

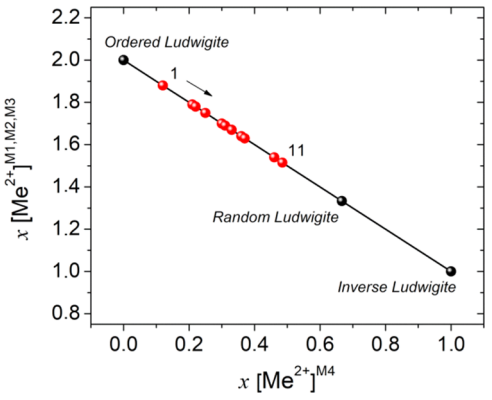

Figure 7. Inversion degree x for the ludwigites. The red symbols show the experimental values of the x. The straight line is drawn by the eye. The numbering corresponds to the increase in the inversion degree: 1. Mg_2FeBO_5,[38] 2. Mg_2InBO_5,[36] 3. Co_2FeBO_5,[19] 4. Ni_2VBO_5,[39] 5. Cu_2GaBO_5,[40] 6. $Co_{2.38}Al_{0.62}BO_5$,[23] 7. Cu_2FeBO_5,[41] 8. Ni_2AlBO_5,[28] 9. Cu_2AlBO_5,[28] 10. Co_2AlBO_5,[28] 11. Co_2AlBO_5 (p.w).

play a crucial role in cationic disorder. There is a sense that electronegativity is precisely the parameter that can influence the cationic distribution and be controlled in the synthesis and design of these compounds. The oxygen prefers to share its electrons with more electronegative cations, Ni^{2+}, Cu^{2+}, Co^{2+}, Fe^{3+}, Ga^{3+}, and especially Sn^{4+}, Ge^{4+}, thus strengthening covalent bonding. Such cations by occupying the M4 site result in the effective holding back of the polymerization of the BO_3 groups, enriching the borate structure. This guess is confirmed by our DFT + U calculations of the electron structure of $Co_{2.5}Ge_{0.5}BO_5$, where the Ge−O bonding was found to be more covalent than that of Co−O and commensurate with B−O one.[30] The less electronegative Al^{3+} or Sc^{3+} is assumed to be squeezed from this site. The M4 site occupation factor (S.O.F.) as a function of the cation's electronegativity is presented in Figure 8. The concentration of the Me^{3+}(Me^{4+}) cation increases as its electronegativity increases. This leads to a decrease in the degree of inversion and, hence, a decrease in the cation disorder. We assume that by combining different

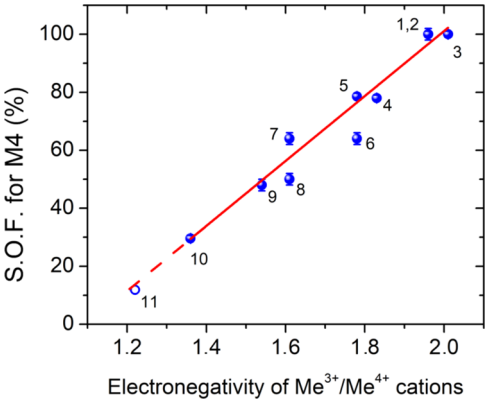

Figure 8. M4 site occupation factor as a function of the cation's Pauling electronegativity in ludwigite structure. The full symbols denote the X-ray diffraction data, and the empty symbols show the predicted yttrium-containing ludwigite. The straight line is a linear approximation. 1. $Co_5SnB_2O_{10}$,[44] 2. $Mg_5SnB_2O_{10}$,[45] 3. $Co_{2.5}Ge_{0.5}BO_5$,[30] 4. Mg_2FeBO_5,[38] 5. Mg_2InBO_5,[36] 6. Co_2InBO_5,[46] 7. Ni_2AlBO_5,[28] 8. Co_2AlBO_5 (p.w.), 9. $Co_5TiB_2O_{10}$,[47] 10. $Co_{2.5}Sc_{0.5}BO_5$,[43] 11. Me_2YBO_5.

electronegativity metals one can obtain ludwigites with different cationic distributions. Mg_2FeBO_5 and Ni_2ScBO_5 are proposed to be candidates for *ordered* and *random* ludwigites, respectively. There is strong experimental evidence from X-ray and Mössbauer spectroscopy measurements to support the smallest degree inversion in Mg_2FeBO_5, x = 0.13.[38,42] To the best of our knowledge, an investigation of Ni_2ScBO_5 has not been reported; however, one might anticipate that such a study would be particularly useful for verifying whether the proposed model is indeed valid. We have grown the $Co_{2.5}Sc_{0.5}BO_5$ single crystals.[43] Although the full substitution was not achieved, the crystal structure refinement showed the statistical distribution of Co^{2+} and Sc^{3+} ions over inequivalent metal sites, supporting the above hypothesis. Reasoning further, the yttrium-containing ludwigite, if it is obtained, can be considered a candidate for the inversion ludwigite.

Intuitively, one can expect that a more electronegative cation would cause a redistribution of the electron density at the M4 site, shifting it toward a more electronegative atom and changing the strength of the interatomic orbital overlap. This may cause a change in the hopping energy t, which describes hybridization between these orbitals, and in electrical conductivity in general. In addition to the covalent bonding effect, filling the M4 site with more electronegative cations favors a low-coordination structure with high barriers to the structure rearrangement. This can explain recent experiments on the annealing of Cu_2FeBO_5 in a reducing atmosphere,[48] which revealed a continuous collapse-recrystallization process without destroying the ludwigite structure. During annealing, Cu^{2+} ions at the M1, M2, and M3 sites are exfoliated, allowing a rearrangement of the structure of the same type, but with Fe^{2+} cations: $Cu_2FeBO_5 \rightarrow Fe_3BO_5$.

5. CONCLUSIONS

Co_2AlBO_5 single crystals were synthesized by using flux. The effects of cationic disorder on structural, magnetic, and electronic properties were studied using X-ray diffraction, *dc* magnetization, and electrical resistivity measurements. The Al^{3+} ions occupying the M1, M2, and M3 sites push the Co^{2+} ions into the M4 site, increasing the degree of inversion up to $x \approx 0.5$. The cationic disorder causes enhancement of the antiferromagnetic correlations, progressive compensation of the magnetic moments along the b-axis, and magnetic softness. The compound exhibits a high magnetic anisotropy. At T_1 = 41 K, the long-range magnetic order onsets, and at T_2 = 20 K, the hysteresis loop opens, implying that a noncompensated magnetic moment appears. The Al substitution results in an increase in the electrical resistivity compared with that of Co_3BO_5, revealing that cation disorder affects hopping mobility. The key to understanding cationic disorder in ludwigites is the crystal structure containing metal and oxygen positions with a large amplitude of displacement. One can conclude that these systems are somewhat predisposed to disorder and that this disorder might be tuned through the exploitation of the structural chemistry of this broad borate family.

■ ASSOCIATED CONTENT

Supporting Information

The Supporting Information is available free of charge at https://pubs.acs.org/doi/10.1021/acs.cgd.4c00582.

https://doi.org/10.1021/acs.cgd.4c00582
Cryst. Growth Des. XXXX, XXX, XXX−XXX

Photo of the Co_2AlBO_5 single crystal, fractional atomic coordinates and equivalent isotropic displacement parameters, anisotropic displacement parameters, main bond lengths, interionic distances Me−Me and average bond angles Me−O−Me, and X-ray microfluorescence mapping of some elements (PDF)

Accession Codes

CCDC 2348879 contains the supplementary crystallographic data for this paper. These data can be obtained free of charge via www.ccdc.cam.ac.uk/data_request/cif, by emailing data_request@ccdc.cam.ac.uk, or by contacting The Cambridge Crystallographic Data Centre, 12 Union Road, Cambridge CB2 1EZ, UK; fax: +44 1223 336033.

AUTHOR INFORMATION

Corresponding Authors

Yulia S. Gokhfeld − *Kirensky Institute of Physics, Federal Research Center KSC SB RAS, Krasnoyarsk 660036, Russia;* orcid.org/0009-0009-8139-2029; Email: yugo@iph.krasn.ru

Natalia V. Kazak − *Kirensky Institute of Physics, Federal Research Center KSC SB RAS, Krasnoyarsk 660036, Russia;* orcid.org/0000-0002-5160-7342; Email: nat@iph.krasn.ru

Authors

Anastasia S. Tarasova − *Siberian Federal University, Krasnoyarsk 660041, Russia*

Alexander D. Vasiliev − *Kirensky Institute of Physics, Federal Research Center KSC SB RAS, Krasnoyarsk 660036, Russia; Siberian Federal University, Krasnoyarsk 660041, Russia*

Evgeniy V. Eremin − *Kirensky Institute of Physics, Federal Research Center KSC SB RAS, Krasnoyarsk 660036, Russia; Siberian Federal University, Krasnoyarsk 660041, Russia*

Andrey A. Borus − *Kirensky Institute of Physics, Federal Research Center KSC SB RAS, Krasnoyarsk 660036, Russia*

Oleg A. Kondratev − *National Research Centre "Kurchatov Institute", Moscow 123182, Russia*

Anna O. Belyaeva − *National Research Centre "Kurchatov Institute", Moscow 123182, Russia;* orcid.org/0009-0006-0536-3371

Sergey G. Ovchinnikov − *Kirensky Institute of Physics, Federal Research Center KSC SB RAS, Krasnoyarsk 660036, Russia; Siberian Federal University, Krasnoyarsk 660041, Russia*

Complete contact information is available at: https://pubs.acs.org/10.1021/acs.cgd.4c00582

Author Contributions

The manuscript was written through contributions of all authors. All authors have given approval to the final version of the manuscript.

Funding

This research was supported by the Russian Science Foundation and Krasnoyarsk Regional Fund of Science and Technology Support, Grant No. 24-12-20012, https://rscf.ru/project/24-12-20012/.

Notes

The authors declare no competing financial interest.

ACKNOWLEDGMENTS

The Co_2AlBO_5 single crystals were grown using a flux developed by the late Leonard Bezmaternykh. X-ray diffraction and magnetization measurements were carried out in the Common Access Facility Centre of SB RAS (Krasnoyarsk, Russia).

REFERENCES

(1) Ramirez, A. P. Strongly Geometrically Frustrated Magnets. *Annu. Rev. Mater. Sci.* **1994**, *24* (1), 453−480.

(2) Kageyama, H.; Yoshimura, K.; Stern, R.; Mushnikov, N. V.; Onizuka, K.; Kato, M.; Kosuge, K.; Slichter, C. P.; Goto, T.; Ueda, Y. Exact Dimer Ground State and Quantized Magnetization Plateaus in the Two-Dimensional Spin System $SrCu_2(BO_3)_2$. *Phys. Rev. Lett.* **1999**, *82* (15), 3168−3171.

(3) Götze, O.; Farnell, D. J. J.; Bishop, R. F.; Li, P. H. Y.; Richter, J. Heisenberg Antiferromagnet on the Kagome Lattice with Arbitrary Spin: A Higher-Order Coupled Cluster Treatment. *Phys. Rev. B* **2011**, *84* (22), No. 224428.

(4) He, J.; Tritt, T. M. Advances in Thermoelectric Materials Research: Looking Back and Moving Forward. *Science* **2017**, *357* (6358), No. eaak9997.

(5) Gascoin, F.; Maignan, A. Order-Disorder Transition in $AgCrSe_2$: A New Route to Efficient Thermoelectrics. *Chem. Mater.* **2011**, *23* (10), 2510−2513.

(6) Cowley, R. A.; Gvasaliya, S. N.; Lushnikov, S. G.; Roessli, B.; Rotaru, G. M. Relaxing with Relaxors: A Review of Relaxor Ferroelectrics. *Adv. Phys.* **2011**, *60* (2), 229−327.

(7) Shvartsman, V. V.; Lupascu, D. C. Lead-Free Relaxor Ferroelectrics. *J. Am. Ceram. Soc.* **2012**, *95* (1), 1−26.

(8) Chen, I. W. Structural Origin of Relaxor Ferroelectrics—Revisited. *J. Phys. Chem. Solids* **2000**, *61* (2), 197−208.

(9) Sofronova, S.; Nazarenko, I. Ludwigites: From Natural Mineral to Modern Solid Solutions. *Cryst. Res. Technol.* **2017**, *52* (4), No. 1600338.

(10) Mir, M.; Guimarães, R. B.; Fernandes, J. C.; Continentino, M. A.; Doriguetto, A. C.; Mascarenhas, Y. P.; Ellena, J.; Castellano, E. E.; Freitas, R. S.; Ghivelder, L. Structural Transition and Pair Formation in $Fe_3O_2BO_3$. *Phys. Rev. Lett.* **2001**, *87* (14), No. 147201.

(11) Larrea, J. J.; Sánchez, D. R.; Litterst, F. J.; Baggio-Saitovitch, E. M.; Fernandes, J. C.; Guimarães, R. B.; Continentino, M. A. Magnetism and Charge Ordering in $Fe_3O_2BO_3$ Studied by ^{57}Fe Mössbauer Spectroscopy. *Phys. Rev. B* **2004**, *70* (17), No. 174452.

(12) Bordet, P.; Suard, E. Magnetic Structure and Charge Ordering in Fe_3BO_5: A Single-Crystal x-Ray and Neutron Powder Diffraction Study. *Phys. Rev. B* **2009**, *79* (14), No. 144408.

(13) Freitas, D. C.; Continentino, M. A.; Guimarães, R. B.; Fernandes, J. C.; Ellena, J.; Ghivelder, L. Structure and Magnetism of Homometallic Ludwigites: $Co_3O_2BO_3$ versus $Fe_3O_2BO_3$. *Phys. Rev. B* **2008**, *77* (18), No. 184422.

(14) Freitas, D. C.; Medrano, C. P. C.; Sanchez, D. R.; Regueiro, M. N.; Rodríguez-Velamazán, J. A.; Continentino, M. A. Magnetism and Charge Order in the Ladder Compound $Co_3O_2BO_3$. *Phys. Rev. B* **2016**, *94* (17), No. 174409.

(15) Bartolomé, J.; Arauzo, A.; Kazak, N. V.; Ivanova, N. B.; Ovchinnikov, S. G.; Knyazev, Y. V.; Lyubutin, I. S. Uniaxial Magnetic Anisotropy in $Co_{2.25}Fe_{0.75}O_2BO_3$ Compared to $Co_3O_2BO_3$ and $Fe_3O_2BO_3$ Ludwigites. *Phys. Rev. B* **2011**, *83* (14), No. 144426.

(16) Galdino, C. W.; Freitas, D. C.; Medrano, C. P. C.; Tartaglia, R.; Rigitano, D.; Oliveira, J. F.; Mendonca, A. A.; Ghivelder, L.; Continentino, M. A.; Sanchez, D. R.; Granado, E. Magnetic, Electronic, Structural, and Thermal Properties of the $Co_3O_2BO_3$ Ludwigite in the Paramagnetic State. *Phys. Rev. B* **2019**, *100* (16), No. 165138.

(17) Kazak, N. V.; Platunov, M. S.; Knyazev, Y. V.; Molokeev, M. S.; Gorev, M. V.; Ovchinnikov, S. G.; Pchelkina, Z. V.; Gapontsev, V. V.; Streltsov, S. V.; Bartolomé, J.; Arauzo, A.; Yumashev, V. V.; Gavrilkin,

S. Y.; Wilhelm, F.; Rogalev, A. Spin State Crossover in Co_3BO_5. *Phys. Rev. B* **2021**, *103* (9), No. 094445.
(18) Kazak, N.; Arauzo, A.; Bartolomé, J.; Molokeev, M.; Dudnikov, V.; Solovyov, L.; Borus, A.; Ovchinnikov, S. Anisotropic Thermal Expansion and Electronic Transitions in the Co_3BO_5 Ludwigite. *Dalton Trans.* **2022**, *51* (16), 6345−6357.
(19) Knyazev, Y. V.; Kazak, N. V.; Zhandun, V. S.; Bartolomé, J.; Arauzo, A.; Belskaya, N. A.; Bayukov, O. A.; Bezmaternykh, L. N.; Ovchinnikov, S. G. Electronic and Magnetic States of Fe Ions in Co_2FeBO_5. *Dalton Trans.* **2021**, *50* (28), 9735−9745.
(20) Fernandes, J. C.; Guimarães, R.; Continentino, M.; Borges, H.; et al. Magnetic Interactions in the Ludwigite $Ni_2FeO_2BO_3$. *Phys. Rev. B* **1998**, *58* (1), 287−292.
(21) Moshkina, E.; Ritter, C.; Eremin, E.; Sofronova, S.; Kartashev, A.; Dubrovskiy, A.; Bezmaternykh, L. Magnetic Structure of Cu_2MnBO_5 Ludwigite: Thermodynamic, Magnetic Properties and Neutron Diffraction Study. *J. Phys.: Condens. Matter* **2017**, *29* (24), No. 245801.
(22) Damay, F.; Sottmann, J.; Lainé, F.; Chaix, L.; Poienar, M.; Beran, P.; Elkaim, E.; Fauth, F.; Nataf, L.; Guesdon, A.; Maignan, A.; Martin, C. Magnetic Phase Diagram for $Fe_{3-x}Mn_xBO_5$. *Phys. Rev. B* **2020**, *101* (9), No. 094418.
(23) Medrano, C. P. C.; Freitas, D. C.; Passamani, E. C.; Pinheiro, C. B.; Baggio-Saitovitch, E.; Continentino, M. A.; Sanchez, D. R. Field-Induced Metamagnetic Transitions and Two-Dimensional Excitations in Ludwigite $Co_{4.76}Al_{1.24}(O_2BO_3)_2$. *Phys. Rev. B* **2017**, *95* (21), No. 214419.
(24) Kumar, J.; Panja, S. N.; John, D.; Bhattacharyya, A.; Nigam, A. K.; Nair, S. Reentrant Superspin Glass State and Magnetization Steps in the Oxyborate Co_2AlBO_5. *Phys. Rev. B* **2017**, *95* (14), No. 144409.
(25) Sheldrick, G. M. SHELXT - Integrated Space-Group and Crystal-Structure Determination. *Acta Crystallogr., Sect. A* **2015**, *71* (1), 3−8.
(26) Sheldrick, G. M. Crystal Structure Refinement with SHELXL. *Acta Crystallogr., Sect. C* **2015**, *71* (1), 3−8.
(27) Burkov, A. T.; Heinrich, A.; Konstantinov, P. P.; Nakama, T.; Yagasaki, K. Experimental Set-up for Thermopower and Resistivity Measurements at 100−1300 K. *Meas. Sci. Technol.* **2001**, *12* (3), 264−272.
(28) Hriljac, J. A.; Brown, R. D.; Cheetham, A. K.; Satek, L. C. The Synthesis and Crystal Structures of the Related Series of Aluminoborates: $Co_{2.1}Al_{0.9}BO_5$, Ni_2AlBO_5, and Cu_2AlBO_5. *J. Solid State Chem.* **1990**, *84* (2), 289−298.
(29) Cohen, M. H.; Reif, F. Quadrupole Effects in Nuclear Magnetic Resonance Studies of Solids. *Solid State Phys.* **1957**, *5*, 321−438.
(30) Kazak, N.; Arauzo, A.; Bartolomé, J.; Belskaya, N.; Vasiliev, A.; Velikanov, D.; Eremin, E.; Gavrilkin, S.; Zhandun, V.; Patrin, G.; Ovchinnikov, S. Temperature- and Field-Induced Transformation of the Magnetic State in $Co_{2.5}Ge_{0.5}BO_5$. *Inorg. Chem.* **2022**, *61* (33), 13034−13046.
(31) Bain, G. A.; Berry, J. F. Diamagnetic Corrections and Pascal's Constants. *J. Chem. Educ.* **2008**, *85* (4), 532−536.
(32) Hoffmann, M.; Dey, K.; Werner, J.; Bag, R.; Kaiser, J.; Wadepohl, H.; Skourski, Y.; Abdel-Hafiez, M.; Singh, S.; Klingeler, R. Magnetic Phase Diagram, Magnetoelastic Coupling, and Grüneisen Scaling in $CoTiO_3$. *Phys. Rev. B* **2021**, *104* (1), No. 014429.
(33) Susuki, T.; Kurita, N.; Tanaka, T.; Nojiri, H.; Matsuo, A.; Kindo, K.; Tanaka, H. Magnetization Process and Collective Excitations in the S = 1/2 Triangular-Lattice Heisenberg Antiferromagnet $Ba_3CoSb_2O_9$. *Phys. Rev. Lett.* **2013**, *110* (26), No. 267201.
(34) Galdino, C. W.; Freitas, D. C.; Medrano, C. P. C.; Sanchez, D. R.; Tartaglia, R.; Rabello, L. P.; Mendonça, A. A.; Ghivelder, L.; Continentino, M. A.; Zapata, M. J. M.; Pinheiro, C. B.; Azevedo, G. M.; Rodríguez-Velamazán, J. A.; Garbarino, G.; Núñez-Regueiro, M.; Granado, E. Structural and Spectroscopic Investigation of the Charge-Ordered, Short-Range Ordered, and Disordered Phases of the $Co_3O_2BO_3$ Ludwigite. *Phys. Rev. B* **2021**, *104* (19), No. 195151.
(35) Damay, F.; Sottmann, J.; Fauth, F.; Suard, E.; Maignan, A.; Martin, C. High Temperature Spin-Driven Multiferroicity in Ludwigite Chromocuprate Cu_2CrBO_5. *Appl. Phys. Lett.* **2021**, *118* (19), No. 192903.
(36) Li, H. K.; Wang, L.; Cai, G. M.; Fan, J. J.; Fan, X.; Jin, Z. P. Synthesis and Crystal Structure of a Novel Ludwigite Borate: Mg_2InBO_5. *J. Alloys Compd.* **2013**, *575*, 104−108.
(37) Brown, I. D.; Altermatt, D. Bond-valence Parameters Obtained from a Systematic Analysis of the Inorganic Crystal Structure Database. *Acta Crystallogr., Sect. B* **1985**, *41* (4), 244−247.
(38) Wiedenmann, A.; Burlet, P.; Chevalier, R. Mössbauer Study of Imperfect One Dimensional Magnetic Systems $FeMgBO_4$ and $FeMg_2BO_5$. *J. Magn. Magn. Mater.* **1980**, *15−18*, 216−218.
(39) Norrestam, R.; Kritikos, M.; Nielsen, K.; Søtofte, I.; Thorup, N. Structural Characterizations of Two Synthetic Ni-Ludwigites, and Some Semiempirical EHTB Calculations on the Ludwigite Structure Type. *J. Solid State Chem.* **1994**, *111* (2), 217−223.
(40) Schaefer, J.; Bluhm, K. Zur Kristallstruktur von $Cu_2M(BO_3)O_2$ ($M = Fe^{3+}$, Ga^{3+}). *J. Inorg. Gen. Chem.* **1995**, *621* (4), 571−575.
(41) Gokhfeld, Y. S.; Kazak, N. V.; Bel'skaya, N. A.; Molokeev, M. S.; Gudim, I. A.; Kondratiev, O. A.; Eremin, E. V.; Knyazev, Y. V.; Velikanov, D. A.; Ovchinnikov, S. G. Structural Disorder, Specific Heat, and Magnetic Transitions in Cu_2FeBO_5. *J. Exp. Theor. Phys.* **2023**, *137* (4), 494−505.
(42) Neuendorf, H.; Gunßer, W. Transition from Quasi-One-Dimensional to Spin-Glass Behaviour in Insulating $FeMg_2BO_5$. *J. Magn. Magn. Mater.* **1997**, *173* (1−2), 117−125.
(43) The Cambridge Crystallographic Data Centre. CCDC Number 2350990. https://www.ccdc.cam.ac.uk/.
(44) Medrano, C. P. C.; Freitas, D. C.; Sanchez, D. R.; Pinheiro, C. B.; Eslava, G. G.; Ghivelder, L.; Continentino, M. A. Nonmagnetic Ions Enhance Magnetic Order in the Ludwigite $Co_5Sn(O_2BO_3)_2$. *Phys. Rev. B* **2015**, *91* (5), No. 054402.
(45) Kawano, T.; Yamane, H. Synthesis, Crystal Structure Analysis, and Photoluminescence of Ti^{4+}-Doped $Mg_5SnB_2O_{10}$. *Chem. Mater.* **2010**, *22* (21), 5937−5944.
(46) Mariano, D. L.; Candela, D. R. S.; Freitas, D. C.; Trujillo, A. Z.; Passamani, E. C.; Continentino, M. A.; Ghivelder, L. Increasing the Magnetic Order Temperature in $Co_3O_2BO_3$:In Ludwigite. *Inorg. Chem.* **2023**, *62* (44), 18040−18048.
(47) Freitas, D. C.; Guimarães, R. B.; Sanchez, D. R.; Fernandes, J. C.; Continentino, M. A.; Ellena, J.; Kitada, A.; Kageyama, H.; Matsuo, A.; Kindo, K.; Eslava, G. G.; Ghivelder, L. Structural and Magnetic Properties of the Oxyborate $Co_5Ti(O_2BO_3)_2$. *Phys. Rev. B* **2010**, *81* (2), No. 024432.
(48) Martin, C.; Maignan, A.; Guesdon, A.; Lainé, F.; Lebedev, O. I. Topochemical Approach for Transition-Metal Exchange Assisted by Copper Extrusion: From Cu_2FeBO_5 to Fe_3BO_5. *Inorg. Chem.* **2017**, *56* (5), 2375−2378.

https://doi.org/10.1021/acs.cgd.4c00582
Cryst. Growth Des. XXXX, XXX, XXX−XXX